Available online at www.sciencedirect.com
SCIENCE DIRECT
Computers and Electronics in Agriculture 46 (2005) 351–378
Computers and electronics in agriculture
www.elsevier.com/locate/compag

Apparent soil electrical conductivity mapping as an agricultural management tool in arid zone soils

S.M. Lesch[a,*], D.L. Corwin[a], D.A. Robinson[b]

[a] *USDA-ARS, George E. Brown Jr. Salinity Laboratory, 450 W. Big Springs Rd., Riverside, CA 92507, USA*
[b] *Department of Plants, Soils and Biometerology, Old Main Hill 4820, Utah State University, Logan, UT 84322, USA*

Abstract

Electromagnetic induction (EM) is a commonly used tool for non-invasive mapping of apparent soil electrical conductivity (EC_a). In this paper, we examine three applications of EM surveying used in arid southwestern US agriculture: repetitive salinity mapping, soil texture mapping, and locating buried tile lines. The basic statistical modeling techniques associated with each application are described and then demonstrated using data from three different field survey projects. In the first study, pre- and post-EM surveys are used to quantify the degree of salt removal from a field leaching event. These survey results demonstrate that the degree of salt removal was spatially variable and that the leaching process was not successful in sub-areas of the field that exhibited high pre-survey salinity concentration levels. The second study demonstrates the use of EM survey data for precision soil texture mapping under non-saline conditions, and illustrates how texture prediction maps can be generated from EM survey data. The final study represents an example of how EM survey data can be used to precisely locate the positions of buried tile lines. In this latter study, two different EM survey data sets that were collected 1 year apart produced estimates of tile line positions within 1 m of each other, validating the reliability and repeatability of the proposed tile line identification strategy. These projects demonstrate three

Abbreviations: EC_a, apparent soil electrical conductivity; EM, electromagnetic induction; H_i, magnetic field; H_p, primary magnetic field; Tx, transmitting coil; Rx, receiving coil; EM_V, vertical EM sensor reading; EM_H, horizontal EM sensor reading; ANOCOVA, analysis of covariance

* Corresponding author.
E-mail address: slesch@ussl.ars.usda.gov (S.M. Lesch).

0168-1699/$ – see front matter. Published by Elsevier B.V.
doi:10.1016/j.compag.2004.11.007

applications of EC_a surveying techniques used to derive spatial information that aids in the effective management of agricultural fields.
Published by Elsevier B.V.

Keywords: Electrical conductivity; EM38; Salinity; Leaching; Tile lines; Regression; ANOCOVA

1. Introduction

Spatial maps of soil properties are invaluable in agriculture for assessing soil quality, planning land use, and determining the suitability of cropping patterns. Apparent soil electrical conductivity (EC_a) survey information has been widely used in agriculture to measure various soil physico-chemical properties. Techniques for predicting soil salinity from EC_a survey data have been discussed by numerous authors, including Williams and Baker (1982), Rhoades et al. (1989, 1999), Hendrickx et al. (1992), Rhoades (1992, 1996), and Lesch et al. (1995a). Other soil properties that have also been successfully mapped using EC_a data include clay content (Williams and Hoey, 1987), depth to clay layers (Doolittle et al., 1994), and moisture content (Sheets and Hendrickx, 1995; Kachanoski et al., 1988). Additionally, yield potential has been shown to be directly related to EC_a data in many applications (Jaynes et al., 1993; Sudduth et al., 1995; Kitchen et al., 1999; Johnson et al., 2003).

The intensive spatial information acquired from a typical EC_a survey is uniquely suited for supplying comprehensive feedback on various agricultural management practices, as well as detailed baseline data for precision farming strategies. Rhoades et al. (1997) discussed how EC_a survey information can be used to determine salt loading and field irrigation efficiency and Triantafilis et al. (1998) described a method for estimating deep drainage from EC_a data. Additionally, various authors have discussed the use and/or interpretation of conductivity survey information for precision farming applications (Plant, 2001; Corwin and Lesch, 2003; Johnson et al., 2003; Lesch and Corwin, 2003).

Direct contact four-electrode systems and non-invasive electromagnetic induction meters tend to be the most frequently used survey instruments for acquiring EC_a data. In this paper, we focus on the latter class of instruments, specifically the Geonics EM38 meter.[1] The primary objective is to show three current applications of the use of electromagnetic induction (EM) survey data in arid southwestern US agriculture. These applications include (1) the mapping and monitoring of soil salinity during a reclamation (leaching) event, (2) soil texture mapping and soil type classification, and (3) identifying and locating buried tile lines.

2. Theory

2.1. EM38 principals of operation

A schematic diagram of the EM38 and its associated electromagnetic fields is presented in Fig. 1. A primary magnetic field (H_p) is induced from a transmitting coil (Tx) at one end

[1] Mention of trademark or proprietary products in this manuscript does not constitute a guarantee or warranty of the product by the U.S. Department of Agriculture and does not imply its approval to the exclusion of other products that may also be suitable.

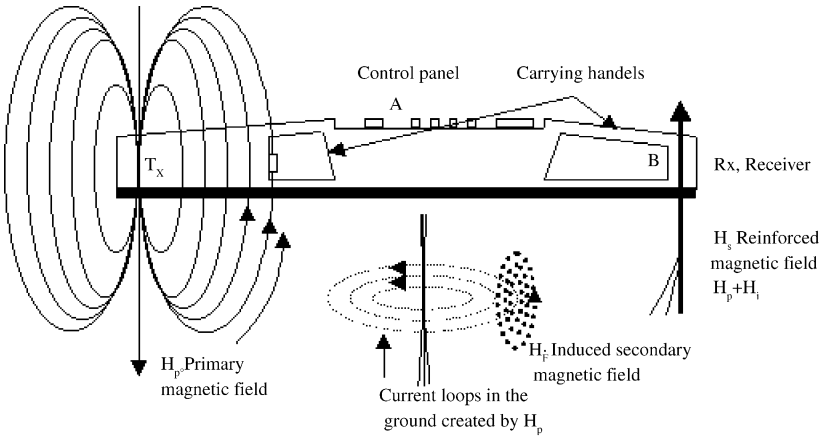

Fig. 1. Diagram of an EM38 meter showing the principles of operation.

of the sensor, this field creates current loops in the ground below and in turn the current loops induce their own magnetic field (H_i). The induced secondary field is superimposed on the primary field and both H_p and H_i are measured in a receiving coil (Rx) at the other end of the sensor (McNeill, 1980). The measured response reflects a nearly linear function of ground conductivity below about 100 mS/m. The meter is designed to be held (or placed) in either a vertical or horizontal orientation; this orientation in turn controls the signal penetration depth and depth weighting response pattern. In a homogeneous soil profile, the vertical (EM_V) signal penetrates to a depth of 1.5–2 m, while the horizontal (EM_H) signal primarily reflects the more shallow soil zone (0.75–1.0 m).

Although the EM38 is designed to be used manually, it can easily be incorporated into a mobilized surveying system that simultaneously collects geo-referenced coordinate location data using a global positioning system (GPS). Examples of such mobilized soil conductivity assessment (MSCA) systems have been described previously in the literature (Carter et al., 1993; Kitchen et al., 1996; Rhoades et al., 1999). These systems have recently become more common, given the introduction of the dual EM38 system (a combined, two-meter system capable of collecting both EM_V and EM_H data simultaneously). More importantly, these systems facilitate the collection of detailed EC_a information in manageable amounts of time, thus greatly increasing the spatial resolution of the EM survey map(s).

The conversion of EC_a survey data into soil salinity can be performed either statistically or deterministically. The statistical approach relies on targeted sampling strategies and either geostatistical or spatial regression calibration models (Lesch et al., 1995a, 1995b; Lesch, 2005). This approach can also be effectively used to estimate other soil properties from EC_a survey data, provided that calibration soil samples are acquired and the survey data are found to be well correlated with the target soil property of interest. In contrast, deterministic approaches normally use pre-specified functional or deterministic soil conductivity models. Such models generally do not require the collection of calibration soil sample data, but do require accurate site-specific information about secondary soil properties known to influence

soil conductivity, such as soil texture and water content (Rhoades et al., 1989; Lesch and Corwin, 2003). In the discussion that follows, the statistical approach will be emphasized.

2.2. The prediction of soil properties from EM survey data

Site-specific prediction of diverse soil properties from EM survey data can be achieved using statistical calibration and prediction techniques. In the regression-based calibration approach advocated by Lesch et al. (1995a), a suitable regression model is specified that relates the target soil property of interest to a transformed linear combination of conductivity signal data readings and (possibly) trend surface coordinates. One example of such a model would be:

$$y = \beta_0 + \beta_1[z_1] + \beta_2[z_2] + \beta_3[c_X] + \beta_4[c_Y] + \varepsilon \quad (1)$$

where the response variable (y) represents the soil property of interest (i.e., salinity, texture, water content, etc.); $z_1 = (EM_V + EM_H)/2$ and $z_2 = (EM_V - EM_H)/2$ represent the average response and normalized difference of the EM signal data; c_X and c_Y represent the associated coordinate locations; β_j parameters represent empirical regression model coefficients, and ε represents the random error component associated with the model. In Eq. (1), the EM readings are linearly transformed in order to reduce the effects of multicollinearity; a problem that arises whenever the raw signal readings are highly correlated. Such a transformation does not increase the accuracy of the regression model, but it does increase the precision of the standard error estimates associated with the transformed regressor variables (Myers, 1986; Cook and Weisberg, 1999). In certain situations, the EM data may also be log transformed (to make the signal data distributions more symmetric), before this linear transformation is applied.

Eq. (1) relates the response variable (i.e., soil property) to both EM signal and trend surface components, and thus can be viewed as a "signal + trend" model. The trend surface components specified in Eq. (1) are optional, and should only be included if they are found to be necessary (i.e., if the associated parameter estimates are statistically significant or if the inclusion of such components is needed to address an obvious spatial trend in a residual plot, etc.). Additionally, the second transformed signal component (the normalized difference) can also be removed from the model if it is both (i) non-significant, and (ii) the removal of this parameter results in a more accurate prediction model. The most common way to assess prediction accuracy is via a jack-knifing analysis; i.e., by comparing the prediction sum of squares (PRESS) statistics for competing regression models and selecting the model with the smallest PRESS score (Myers, 1986; Cook and Weisberg, 1999). Relying on both sets of statistics for parameter selection is more appropriate (then relying just on significance tests), since the ultimate goal of the modeling process is to identify the best prediction function.

The optimal estimation of the above (or similar) regression model depends on the assumptions placed on the random error component. If the errors are assumed to exhibit spatial correlation, then Eq. (1) is commonly called a spatial linear regression model in the statistical literature, or a kirging with external drift model in the geostatistical literature (Royle and Berliner, 1999). Such models can be efficiently estimated using maximum likelihood or restricted maximum likelihood fitting techniques (Littell et al., 1996). In contrast, if the errors can be assumed to be (at least approximately) independent, then ordinary least squares

(OLS) fitting techniques can be used. In this latter case, the model becomes identical to an ordinary linear regression equation, the only difference being that the predictions are spatially referenced.

The likelihood of the residual errors being approximately independent (as opposed to spatially correlated) depends primarily on (i) the method used to select the calibration sample sites, and (ii) the degree to which the conductivity signal data correlates with the response variable of interest. When the signal data are strongly correlated with the target soil property and specialized sampling strategies are employed, the assumption of approximate residual independence is often satisfied. For a detailed discussion concerning these issues see Lesch (2005).

Although appropriate prediction statistics can be derived for either case, only the OLS results are presented throughout this paper. Individual point and range interval predictions are presented first, and then extended to include the prediction of field average estimates and average range interval estimates. All results are presented in matrix notation; a good review of matrix notation from a regression modeling viewpoint is given in Myers (1986).

2.2.1. Individual point (survey site) predictions

Define $\mathbf{X}$ to be the regression model design matrix, and $\mathbf{x}_i$ to be the regression vector associated with the ith prediction site. Additionally, let $\boldsymbol{b}$ represent the estimated regression parameter vector, and $\hat{y}_i$ represent the (possibly log transformed) predicted soil property at the ith prediction site. The following results can then be derived from standard general linear modeling theory:

$$\hat{y}_i = \mathbf{x}_i'\boldsymbol{b} \tag{2}$$

$$\text{var}(y_i - \hat{y}_i) = \theta^2 = \sigma^2(1 + \mathbf{x}_i'(\mathbf{X}'\mathbf{X})^{-1}\mathbf{x}_i) \tag{3}$$

where $\text{var}(y_i - \hat{y}_i)$ represents the expected prediction variance and σ^2 represents the regression model mean square error (MSE) term (Myers, 1986; Graybill, 1976). Additionally, from a Bayesian perspective, one can view the regression model prediction as a random variable having a mean of $\hat{y}$ and a variance of θ^2, (Press, 1989, assuming a vague prior distribution). In turn, this implies that the probability that y lies within the interval (a, b) can be computed by integrating over a t-distribution from $g_1 = ((a - \hat{y})/\theta)$ to $g_2 = ((b - \hat{y})/\theta)$. Mathematically, this integration can be written as:

$$\pi_{i,[a,b]} = \text{Probability}(a \leq y_i \leq b) = \int_{g_1,g_2} t(n - p)\text{d}t \tag{4}$$

where $t_{(n-p)}$ represents a t-distribution having n–p degrees of freedom (i.e., the regression model residual degrees of freedom). Thus, Eq. (2) represents the regression model point prediction, and Eq. (3) can be used to determine the variance associated with this prediction. Likewise, Eq. (4) can be used to determine the probability that the true soil property level actually lies within the interval (a, b).

If a log transformation has been applied to the soil property being modeled, a back-transformed geometric point estimate can be calculated as:

$$\text{BT-geometric estimate} = \exp(\mathbf{x}_i'\boldsymbol{b}) \tag{5}$$

For example, maps made from back-transformed geometric salinity estimates are referred to as "geometric salinity distribution maps" by Lesch et al. (1995a). If needed, a method-of-moment estimate of the arithmetic point estimate can also be calculated,

$$\text{BT-arithmetic estimate} = \exp(\mathbf{x}_i'\boldsymbol{b} + 0.5\theta^2) \tag{6}$$

2.2.2. Field average prediction estimates

In addition to generating point predictions, a regression model can also be used to make global (field) average estimates. These field summary statistics include the (i) mean estimate of the soil property across the survey grid and (ii) field average range interval estimates associated with the grid.

An average estimate for either the entire survey grid or some specific subsection of the survey grid can be directly calculated via the estimated regression model. Define $\mathbf{x}_{\text{ave}}$ to be the average of the N regression vectors associated with the non-sampled sites on the grid subsection of interest. Then the estimate for the average mean level and associated variance is:

$$\hat{y}_{\text{ave}} = \mathbf{x}_{\text{ave}}'\boldsymbol{b} \tag{7}$$

$$\text{var}(y_{\text{ave}} - \hat{y}_{\text{ave}}) = \theta^2_{\text{ave}} = \sigma^2\left(\frac{1}{N} + \mathbf{x}_{\text{ave}}'(\mathbf{X}'\mathbf{X})^{-1}\mathbf{x}_{\text{ave}}\right) \tag{8}$$

When one or more calibration sample locations fall within the grid subsection, Eq. (8) can be modified to include a finite-correction factor. However, in a typical survey where the number of prediction sites is much larger that the number of calibration sites ($N \gg n$), the effect of such a correction is usually trivial. Note also that Eqs. (7) and (8) implicitly assume that the survey data has been collected uniformly across the area of interest.

Along with the global mean estimate, the proportion of sites on the survey grid with soil property levels above, below, and/or within a specific range is also often of interest. Such estimates are referred to as field average range interval estimates (Lesch et al., 1995a). The previously discussed individual probability intervals can be used to calculate such estimates. These estimates adjust out the "shrinkage effect" inherent in the associated regression model predictions. Mathematically, a range interval estimate (RIE $[a, b]$) for a survey area (for any given range interval with endpoints a and b) can be calculated as:

$$\text{RIE}[a, b] = \left(\frac{100}{N}\right)\left[\sum_{i=1,N}\left(\pi_{i,[a,b]}\right)\right] \tag{9}$$

where $\pi_{i,[a,b]}$ was defined previously in Eq. (4).

The calculation of an exact variance for (9) is extremely difficult, due to the nonlinear nature of the probability interval estimate. However, an approximate variance estimate can be calculated from the jack-knifed REI $[a, b]$ estimates, using the standard jack-knife variance formula (Thompson, 1992). All REI standard error estimates presented in this study have been calculated in this manner.

2.3. Tile line mapping

Cyclic patterns in EM survey data are often observed in many saline or semi-saline agricultural fields, and generally indicate the presence of buried tile lines (Rhoades et al., 1997). Both the reduction in water content and the leaching of salts directly over the tile lines tends to produce a sharp drop-off in the EM signal response. In turn, this produces a cyclic EM conductivity pattern down the transect with the local minimum levels occurring over the tile lines. When a series of linear transects are obtained across a field, these cyclic patterns can be de-trended, analyzed, and used to map out the tile line positions.

The actual mapping of tile lines can be performed by (i) identifying the local minima within the field, (ii) assigning these minima to individual tile lines, and (iii) estimating an appropriately specified analysis of covariance (ANOCOVA) model that algebraically defines the tile line positions in two-dimensional space. Some brief details associated with each step are outlined below.

Step 1: Identifying the local minima.

1.a apply a smoothing algorithm to each vector of EM transect data;

1.b compute the difference between the raw and smoothed EM data (this difference data is referred to as "filtered" data, respectively);

1.c identify the minima positions from the filtered data using a suitable search algorithm.

Step 2: Assignment of the minima to specific tile lines.

2.a using a suitable interactive graphics environment, identify each set of minima that form linear patterns (i.e., lines) across the field;

2.b associate each set of points that form a distinct linear pattern into a common group (this set of points defines a probable tile line).

Step 3: Define and estimate the ANOCOVA model.

3.a Determine the type of line equations that the ANOCOVA model must estimate; i.e., $y = mx + b$ or $x = my + b$.

3.b If the tile lines can be assumed to be parallel, simultaneously estimate the positions of all the tile lines using an ANOCOVA model defined as $z = \alpha_j + \beta(w)$, where (z) represents the coordinate data treated as the response variable, (w) represents the coordinate data used as the predictor variable, the α_j's represent the unique intercepts for the k identified tile lines ($j = 1, \ldots, k$) and β represents the common slope estimate.

The process outlined above has been implemented in the ESAP Software Package, Version 2.30 (Lesch et al., 2000).[2] Equivalently, it can be performed using suitable GIS and statistical software. Numerous filtering techniques can be used in Step 1, but an ordinary moving average estimate should be more than adequate for most situations. Once the filtered EM transect data has been computed, local minimums can be found using a simple search algorithm. In ESAP, a local minimum is defined to be any filtered EM reading that is both negative and consistently lower than each adjacent filtered reading (located to either side of the current reading).

[2] ESAP is public domain software and can be obtained from the George E. Brown Jr. Salinity Laboratory web site (www.ussl.ars.usda.gov).

Step 2.b is referred to as "tile line threading", since a line is essentially threaded through a linear pattern of points. This process is best accomplished in an interactive graphics environment that allows one to manually define a line through each apparent linear pattern. A simple point-to-line distance algorithm can then be used to assign minima to unique lines (i.e., all points that lie within a specific distance to a particular line segment get assigned into the same group).

Once a suitable set of points have been assigned to a series of probable lines, the ANOCOVA model can be used to optimize the apparent tile line locations. The purpose of this analysis is to estimate the tile line equations; these equations can in turn be used to predict coordinate positions in one dimension from their associated positions in the other dimension. For example, if the tile lines run predominantly east–west, then one would adopt the $y = mx + b$ form of the equation and thus predict the y-coordinate from the x-coordinate. Note that a unique intercept is estimated for each line, and the common slope parameter is appropriate if all of the tile lines are assumed to be parallel (this latter assumption can be tested statistically). Outside of re-scaling the GPS coordinate data to avoid possible numerical estimation problems, this estimation technique is carried out exactly like a standard ANOCOVA analysis.

If the tile lines are not laid out parallel to one another, then a unique slope parameter can be incorporated into the ANOCOVA model for each line. Alternatively, if the functional form of the tile line equation changes across lines, then each line can be estimated individually.

3. Materials and methods

Survey data from three fields are presented in this report to demonstrate both soil property and tile line mapping techniques. All of the analyses preformed on these fields (designated as CV5, M22, and IV376) were carried out using the ESAP Software Suite, Versions 2.01 and 2.30 (Lesch et al., 2000) and SAS, Version 8 (SAS Institute Inc., 1999). A site map of the field project locations is shown in Fig. 2; pertinent details concerning each field survey are given below.

3.1. Case study 1 (CV5): pre- versus post-leaching salinity mapping

Field CV5 is a 13 ha agricultural field located in Coachella Valley, CA. This field had been brought back into production in 1999, after sitting idle for approximately 8 years. The NRCS soil classification map (USDA, 1980) for this field indicated the presence of four similar soil types, all consisting of fine to very fine sandy loam surface material and sandy loam subsurface material stratified with silt lenses and silt plates (sandy, mixed hyperthermic Typic Torrifluvents). A winter wheat crop grown in 1999 showed signs of poor growth areas, believed to be due to excessive soil salinity (personal communication, landowner). Due to this yield reduction, the landowner elected to fallow, disk, and leach this field in the summer of 2000, and requested both pre- and post-leaching salinity survey data in order to appraise the leaching process.

Two independent EM/salinity surveys were performed in Field CV5 in May and August, 2000 by Salinity Laboratory and Coachella Valley Resource Conservation District

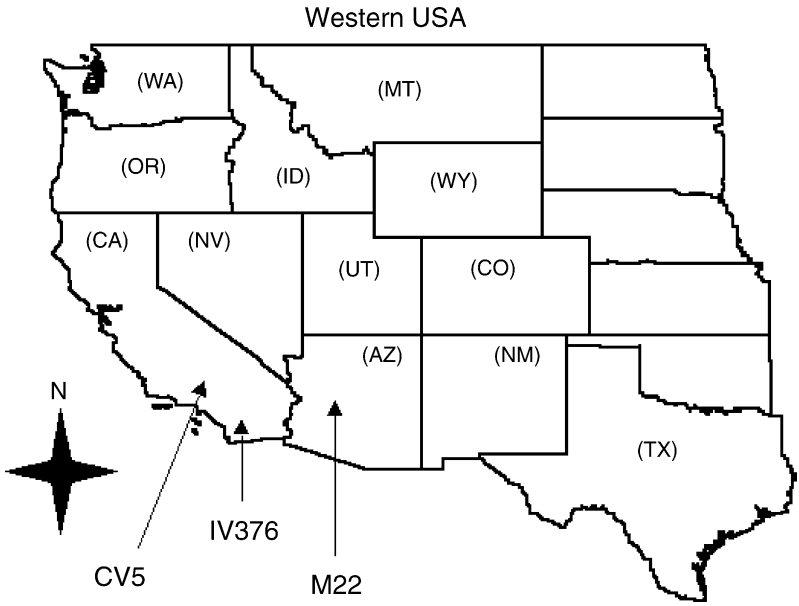

Fig. 2. Site map of California and Arizona field project locations.

personnel. Each survey was performed using a dual EM38 system mounted to a MSCA platform. The pre-leaching survey was performed in May, after the field had been fine disked, laser leveled, and floated. This first survey consisted of 1615 pairs of horizontal and vertical EM38 readings collected across 33 southwest–northeast transects, with each transect spaced approximately 18 m apart. The post-leaching survey was performed in August, approximately 4 weeks after the last cycle of leaching water had infiltrated the soil. This second survey consisted of 1569 pairs of horizontal and vertical EM38 readings collected across 40 east–west transects, with each transect spaced approximately 10 m apart. Co-located differential GPS coordinate information was obtained at all sites during both surveys using a Trimble Pro-XRS GPS system with sub-meter accuracy. Both sets of survey data were independently processed using the ESAP-RSSD software program, and two (non-overlapping) 12 site calibration sampling plans were generated.

The leaching process began approximately 2 weeks after the first survey was completed and continued intermittently for 6 weeks. Approximately 7.9 ha m of Colorado river water (electrical conductivity of the saturation extract (EC_e) $\approx$ 1.1 dS/m) was applied to the field using a sequential, spill-over basin design (i.e., a design where water is flooded into the first basin and allowed to fill adjacent basins via the use of hand operated gates). The basins were approximately 18-m wide and 380-m long, and orientated in a predominantly east–west direction. No evidence of basin erosion was observed during the leaching process. However, about 2 ha m of the applied water was estimated to have evaporated, based on local pan evaporation measurements collected during the same time frame.

Soil cores at 12 distinct sampling locations were collected down to a depth of 1.2 m during both surveys. Each soil core was split into two 60-cm samples and analyzed for

salinity (EC_e, dS/m), soil saturation percentage (SP), and gravimetric soil water content ($2g$, kg/kg). The primary goal of this study was to model the EM/salinity relationship(s) and produce depth-specific pre- versus post-leaching spatial salinity maps and field average statistics (in order to quantify the effectiveness of the leaching process).

3.2. Case study 2 (M22): soil texture (% clay) mapping

Field M22 is a 7-ha experimental research field located at the Maricopa Agricultural Center in Maricopa, Arizona. This field had been used to grow cotton during the previous three growing seasons, and was surveyed by Salinity Laboratory personnel in April, 2002. Immediately before the survey took place, M22 was rough disked and a 1.02 m bed-furrow system had been put in place across the field. These beds were not topped or planted, but the general bed shape was consistent across the field. The near surface (0–30 cm) soil moisture level was well below field capacity, but still sufficient for performing the EM survey.

A total of 2518 pairs of horizontal and vertical EM-38 readings were collected across 57 distinct east–west transects, with each transect spaced 7.1 m (7 rows) apart. Collocated differential GPS coordinate information was obtained at each survey site using a Trimble Pro-XRS GPS system having sub-meter accuracy. This survey data was then processed using the ESAP-RSSD software program, and a 12 site calibration sampling plan was generated. Soil sample cores were retrieved at these 12 sites down to a depth of 90 cm and analyzed for salinity (EC_e, dS/m), soil texture (% sand, silt, and clay), saturation percentage (SP), gravimetric soil water content ($2g$, kg/kg, and cations in the saturation extract (Na, Ca, Mg, K; meq/L).

The primary purpose of the EM survey and soil sampling in Field M22 was to delineate the apparent spatial variation in soil texture across the plot. This field was known a priori to be non-saline and texturally variable, thus we expected the EM survey data to be predominantly influenced by variation in the soil texture and water content levels. The NRCS soil classification map (USDA, 1984) for this field indicated the presence of two soil types; Casa Grande clay loam (fine-loamy, mixed, hyperthermic Typic Natrargids) and Mohall sandy loam (fine-loamy, mixed, hyperthermic, Typic Haplargids), with the Mohall soil type occurring in the north–east portion of the field. Additionally, the presence of both soil types had been confirmed by previous soil sampling studies performed in this field.

3.3. Case study 3 (IV376): tile line mapping

Field IV376 is a 64-ha field located in Imperial Valley, California, that has supported permanent bedded alfalfa since 1999. Multiple EM surveys have been performed in this field since early 2001, as part of a district wide salinity-monitoring program. This field contains 10 tile lines that exhibit a pronounced influence on the apparent magnitude of the spatial EM signal pattern. These tile lines are orientated east to west, and were installed at a depth of 2.44 m. According to the installation records on file at the Imperial Irrigation district, seven east–west lines were originally installed in Field IV376 at a spacing of 106.68 m. Approximately 10 years after the original seven lines were installed, three additional lines were "split" into the northern section of this field (thus reducing the tile line spacing in the northern half of the field to 53.34 m). In this manuscript, we analyze the EM survey data

from two prior surveys (July 2002 and August 2001), and use this data to infer both the precise positions of these lines and the repeatability of the tile line mapping process.

In the August 2001 survey, 7469 EM readings were acquired across 31 distinct north–south EM transects within IV376. These transects were spaced approximately 25 m apart, and distinct EM signal data were acquired approximately every 3.1 m. In the July 2002 survey, 5603 EM readings were acquired across 24 distinct north–south EM transects. These transects were spaced approximately 32 m apart, and EM signal data were acquired approximately every 3.2 m. Since the mapping of tile lines can be done directly from EM survey data, the associated soil salinity calibration sample data from this field will not be discussed. Additionally, only the EM_V signal data is used in the analysis, since the deeper penetrating EM_V signal tends to produce more reliable results in most tile line mapping applications.

4. Results and discussion

4.1. Pre- versus post-leaching salinity study (Field CV5)

Table 1 presents descriptive EM38 summary statistics for both surveys performed in Field CV5. The means and standard deviations of the EM_V and EM_H signal readings are reasonably similar across time frames. The correlation between the vertical and horizontal signal data in each time frame is extremely high ($r \approx 0.98$ in each survey, after applying a natural log transformation). Both the EM vertical and horizontal signal data exhibit marked skewness in each survey data set, as shown by the quantile statistics.

The spatial maps of the pre- versus post-leaching EM survey data look extremely similar. Fig. 3a and b show the observed pre- and post-leaching EM_V signal maps, respectively, along with the locations of the 12 calibration sample sites in each survey process. The similarity in the EM_H signal maps (not shown) is just as striking.

Table 1
EM38 summary statistics for Field CV5, pre- and post-leaching surveys

	Pre-leaching survey		Post-leaching survey	
	EM_V (mS/m)	EM_H (mS/m)	EM_V (mS/m)	EM_H (mS/m)
N	1615	1615	1569	1569
Mean	131.25	93.14	130.38	100.43
Standard deviation	75.94	56.30	87.69	67.13
Quantiles				
Minimum	44.0	26.0	24.0	26.0
q10	60.0	43.0	49.0	43.0
q25	76.0	53.0	64.0	53.0
Median	108.0	74.0	100.0	77.0
q75	166.0	115.0	172.0	129.0
q90	238.0	169.0	253.0	190.0
Maximum	586.0	501.0	712.0	634.0
Correlation				
Corr (ln (EM_V), ln (EM_H))	0.979		0.984	

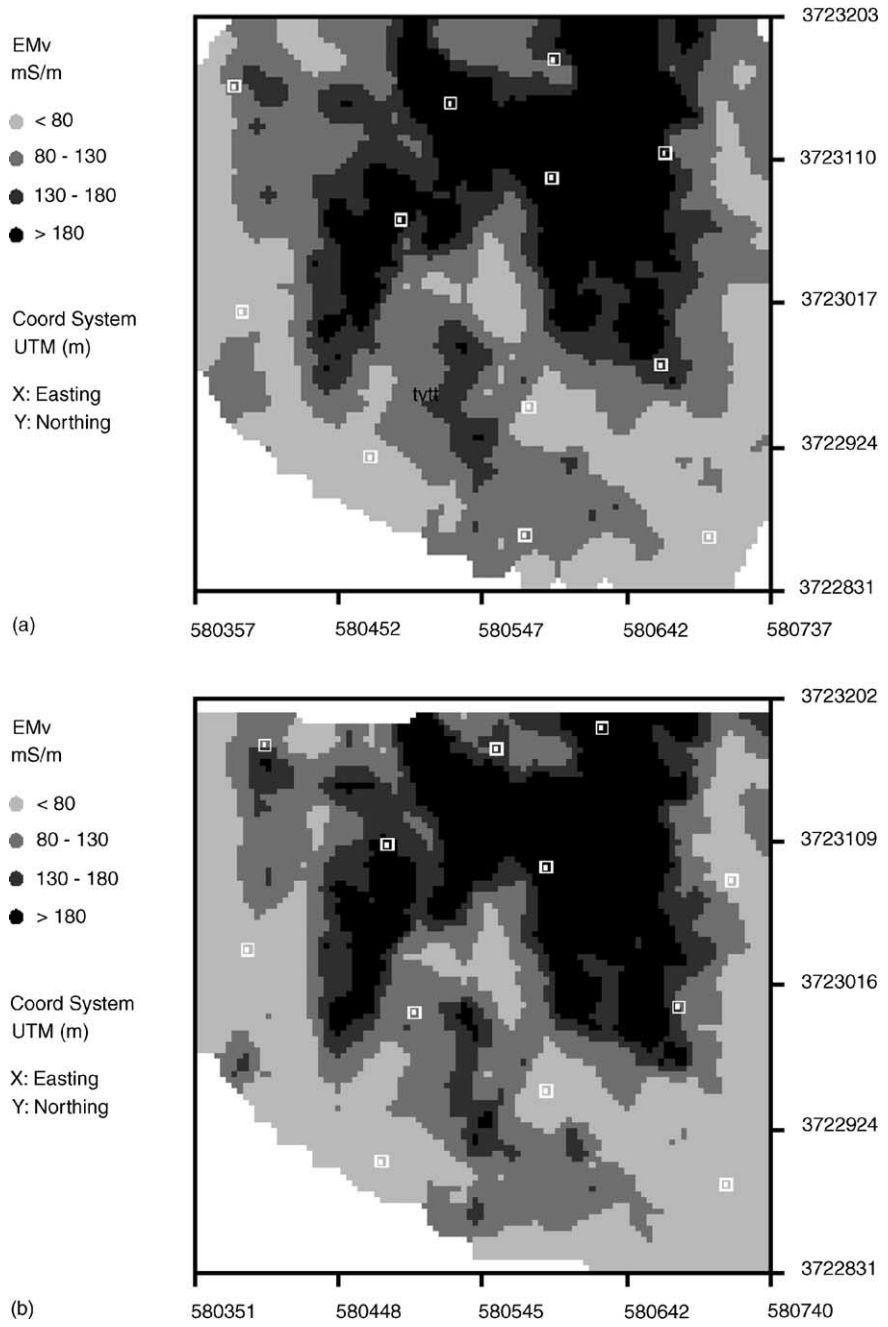

Fig. 3. Observed (a) pre- and (b) post-leaching EM_V signal patterns in Field CV5, with the 12 calibration sample site locations identified for each time frame.

Table 2
Calibration soil sample summary statistics for Field CV5, pre- and post-leaching surveys

Soil Property	Depth level (cm)	Mean	Standard deviation	Minimum	Maximum
Pre-leaching soil sample data statistics					
EC_e (dS/m)	0–60	6.77	9.61	0.68	35.10
	60–120	9.48	11.99	1.28	34.65
SP (%)	0–60	41.09	6.34	33.44	52.42
	60–120	43.56	7.38	31.19	56.78
θ_v (ratio)[a]	0–60	0.216	0.073	0.078	0.308
	60–120	0.311	0.097	0.136	0.409
Post-leaching soil sample data statistics					
EC_e (dS/m)	0–60	4.93	4.86	0.60	13.44
	60–120	8.29	10.62	0.65	39.15
SP (%)	0–60	40.45	5.07	33.67	49.63
	60–120	45.04	8.05	31.12	62.60
θ_v (ratio)	0–60	0.224	0.082	0.095	0.344
	60–120	0.308	0.096	0.158	0.488

[a] Estimated from θ_g and calculated bulk density, where the bulk density was calculated from the measured SP.

Table 2 shows the calibration soil sample summary statistics associated with each survey. These statistics include the mean, standard deviation, minimum and maximum levels for the measured EC_e, SP, and estimated θ_v for the 0–60 and 60–120 cm sampling depths. Like the EM signal data, the salinity data distributions also appeared to be significantly asymmetrical (i.e., right-skewed).

In this study, the goal was to predict the pre- and post-leaching spatial salinity patterns in CV5 from the corresponding EM survey data. Given the clearly asymmetric distributions, we initially fit a log/log regression model defined as:

$$\ln(EC_e) = \beta_0 + \beta_1(w_1) + \beta_2(w_2) + \varepsilon \tag{10.1}$$

to each sample depth and time frame, where $w_1 = (\ln(EM_V) + (\ln(EM_H))/2$ and $w_2 = (\ln(EM_V) - (\ln(EM_H))/2$. However, an assessment of the PRESS scores suggested that the β_2 parameter could be dropped from the post-leaching models, so the post-leaching regression function was redefined to be:

$$\ln(EC_e) = \beta_0 + \beta_1(w_1) + \varepsilon \tag{10.2}$$

The corresponding regression model summary statistics and parameter estimates for Eqs. (10.1) and (10.2) are shown in Table 3. The R^2 values for all four models are between 0.87 and 0.91, suggesting that about 90% of the observed variation in the log salinity data at each sampling depth can be explained by the log transformed EM signal data from each survey.

The four regression models shown in Table 3 were then used to calculate the field summary statistics and range interval estimates using Eqs. (7)–(9) for each sample depth and time frame. These results are shown in Table 4. The individual point predictions were also used to create predicted salinity maps; the 0–60 cm pre- and post-leaching predicted

Table 3
Regression model summary statistics for Field CV5, pre- and post-leaching surveys

	Pre-leaching models		Post-leaching models	
	(0–60 cm)	(60–120 cm)	(0–60 cm)	(60–120 cm)
R^2	0.906	0.870	0.896	0.895
MSE	0.142	0.233	0.148	0.134
Depth	Estimate	Standard error	*t*-Score	Prob > |*t*|
Pre-leaching parameter estimates ($E(y) = \beta_0 + \beta_1 z_1 + \beta_2 z_2$)				
0–60 (cm)				
β_0	−4.49	0.82	−5.50	<.001
β_1	1.38	0.16	8.68	<.001
β_2	3.29	1.53	2.14	0.061
60–120 (cm)				
β_0	−6.10	1.05	−5.83	<.001
β_1	1.58	0.20	7.76	<.001
β_2	−2.22	1.96	−1.14	0.285
Post-leaching parameter estimates ($E(y) = \beta_0 + \beta_1 z_1$)				
0–60 (cm)				
β_0	−5.55	0.72	−7.72	<.001
β_1	1.45	0.16	9.30	<.001
60–120 (cm)				
β_0	−4.66	0.68	−6.81	<.001
β_1	1.37	0.15	9.21	<.001

spatial EC_e maps are shown in Fig. 4a and b, respectively. These field statistics and maps can be used to evaluate the success of the leaching process.

As shown in Table 4, the leaching process slightly lowered the 0–60 cm geometric mean salinity level from an estimated 3.40 to 2.91 dS/m (an 16.8% reduction). Likewise, a similar increase in the 60–120 cm geometric mean salinity level occurred (i.e.,

Table 4
Field average prediction statistics for Field CV5, pre- and post-leaching surveys

Depth (cm)	Pre-leaching survey geo-mean (95% CI)	Post-leaching survey geo-mean (95% CI)	% Change
Predicted field median EC_e levels			
0–60	3.40 (2.66, 4.36)	2.91 (2.27, 3.74)	−16.8
60–120	4.40 (3.21, 6.04)	4.87 (3.85, 6.17)	+9.7

Range (dS/m)	0–60 cm depth estimates		60–120 cm depth estimates	
	Pre-leaching	Post-leaching	Pre-leaching	Post-leaching
Predicted field range interval estimates (with standard errors)				
0–2	28.3 (4.4)	38.6 (4.1)	22.5 (5.7)	17.3 (7.0)
2–4	31.2 (3.0)	25.3 (3.0)	25.9 (3.9)	27.8 (2.5)
4–8	23.8 (2.4)	19.6 (1.8)	24.0 (2.3)	25.3 (3.9)
>8	16.7 (4.5)	16.5 (5.3)	27.6 (5.3)	29.6 (3.1)

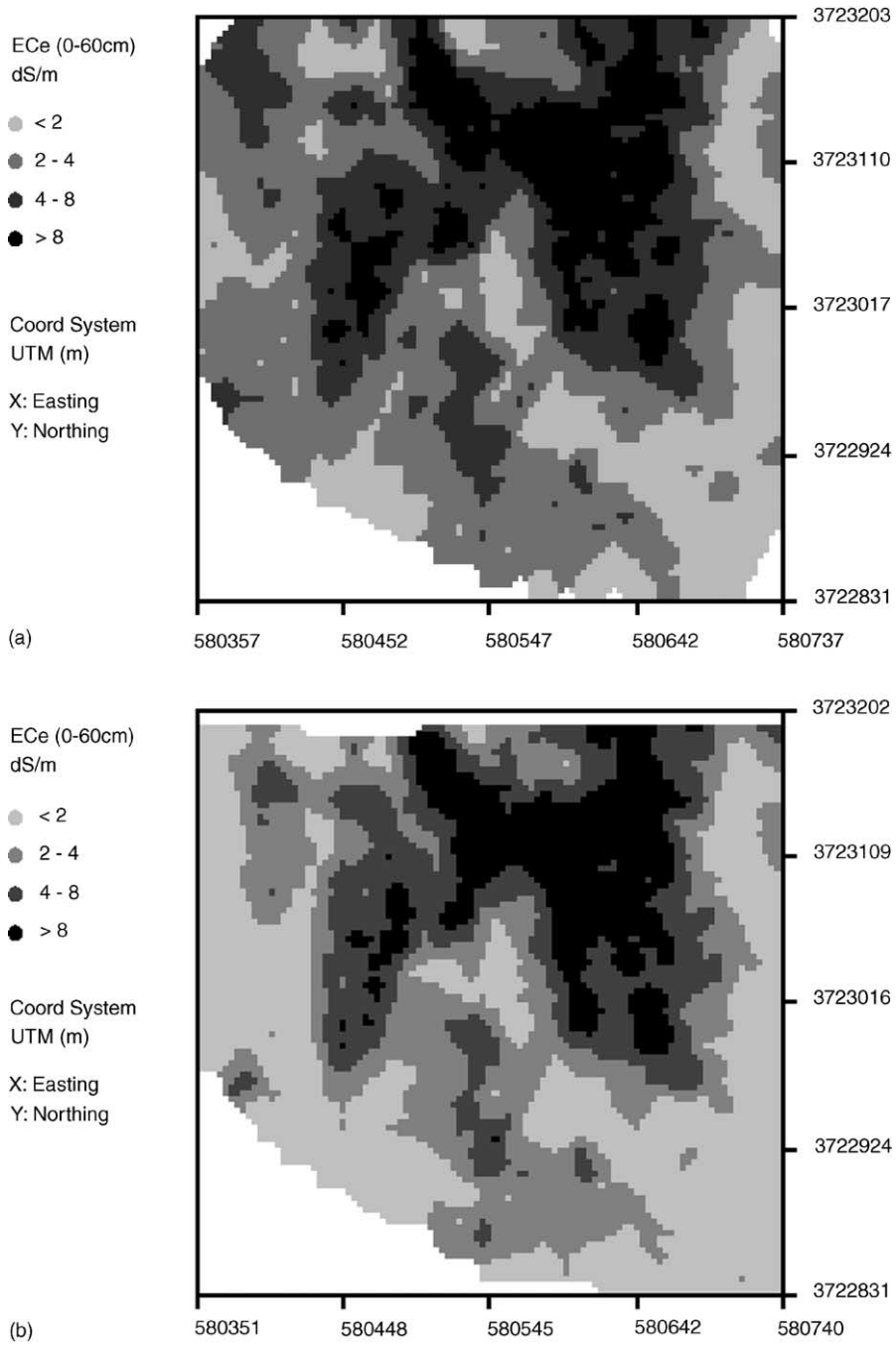

Fig. 4. Predicted (a) pre- and (b) post-leaching salinity maps (0–60 cm) for Field CV5.

from 4.40 to 4.87 dS/m). Two-sample *t*-tests performed on the corresponding log–mean salinity estimates indicate that these predicted changes are not statistically significant (0–60 cm depth: $t = -0.99$, $p = 0.003$; 60–120 cm depth: $t = 0.58$, $p = 0.581$). These results suggest that the apparent average downward redistribution of salt is not statistically meaningful.

The range interval estimates shown in Table 4 better clarify the apparent salt movement. At the 0–60 cm depth, the post-leaching proportion of area classified in the 0–2, 2–4, and 4–8 dS/m ranges are 38.6%, 25.3%, and 19.6%, respectively. The apparent change from the corresponding pre-leaching estimates (28.3%, 31.2%, and 23.8%) suggests that the leaching process primarily impacted the areas in the field with initial salinity levels <8 dS/m. In contrast, the % area estimated to be >8 dS/m did not change in any meaningful manner (i.e., 16.7% versus 16.5%). The changes in the 60–120 cm depth are much less pronounced, although still possibly indicative of a slight salt-loading effect. Approximate Chi-square tests performed on each set of estimates suggest that the changes in the 0–60 cm depth are marginally significant ($\chi^2 = 6.78$, $p = 0.079$), while the apparent changes in the 60–120 cm depth are non-significant ($\chi^2 = 0.70$, $p = 0.873$).

The preferential nature of this leaching process can be clearly seen by comparing the pre- versus post-leaching 0–60 cm predicted salinity maps (Fig. 4a and b, respectively). The two predicted salinity patterns look disturbingly similar, and the areas classified as >8 dS/m appear almost identical. The only noticeable difference between these two maps appears to be the reduction in size of the post-leaching 2–4 dS/m zone (and corresponding increase in the 0–2 dS/m zone).

Overall, these summary statistics and prediction maps suggest that a high degree of preferential leaching occurred in this field. Specifically, nearly all of the downward salt movement appears to have occurred in the less saline areas ($EC_e < 8$ dS/m), while little (if any) movement occurred in the more saline areas. These results imply that the main goal of the leaching process (i.e., the lowering of the salinity levels in the most saline areas) was not achieved.

Why the leaching process failed is not apparent from the survey data. Multiple thin silt lenses were encountered at 60–90 cm in the high saline areas during the calibration sampling; these lenses might have restricted the vertical water flow. Or there may be an impermeable soil layer below 1.2 m in these areas. Further investigation is necessary to resolve this preferential leaching issue. Nonetheless, these results served to alert the landowner to the continued salinity problem and convince him that additional leaching would not be cost effective without performing some type of physical intervention (such as slip-plowing the high saline zones).

4.2. Soil texture mapping (Field M22)

Table 5 presents the EM38 summary statistics for the survey performed in Field M22. Unlike the previous EM38 data collected in CV5, these vertical and horizontal readings are much lower, with means of 84.8 and 40.1 mS/m, respectively. The EM_H signal data appear to be about 50% lower than the collocated EM_V data, probably due to the low moisture levels in the 0–30 cm soil layer. The correlation level between the EM_V and EM_H signal readings is also lower ($r \approx 0.87$), and the data distributions appear to be bimodal.

Table 5
EM38 summary statistics for Field M22

	EM_V (mS/m)	EM_H (mS/m)
N	2518	2518
Mean	84.78	40.09
Standard deviation	6.12	6.68
Quantiles		
Minimum	65.8	16.2
q10	74.7	29.3
q25	82.3	36.6
Median	86.4	41.8
q75	89.0	44.9
q90	91.1	47.1
Maximum	97.0	52.9
Correlation		
Corr (EM_V, EM_H)	0.868	

Fig. 5 shows the spatial map of the EM_H signal data, along with the locations of the 12 calibration sample sites identified from the survey process. This map shows a clearly distinguishable lower conductivity zone in the north-eastern section of the field, which roughly corresponds to the NRCS mapped Mohall sandy loam soil type.

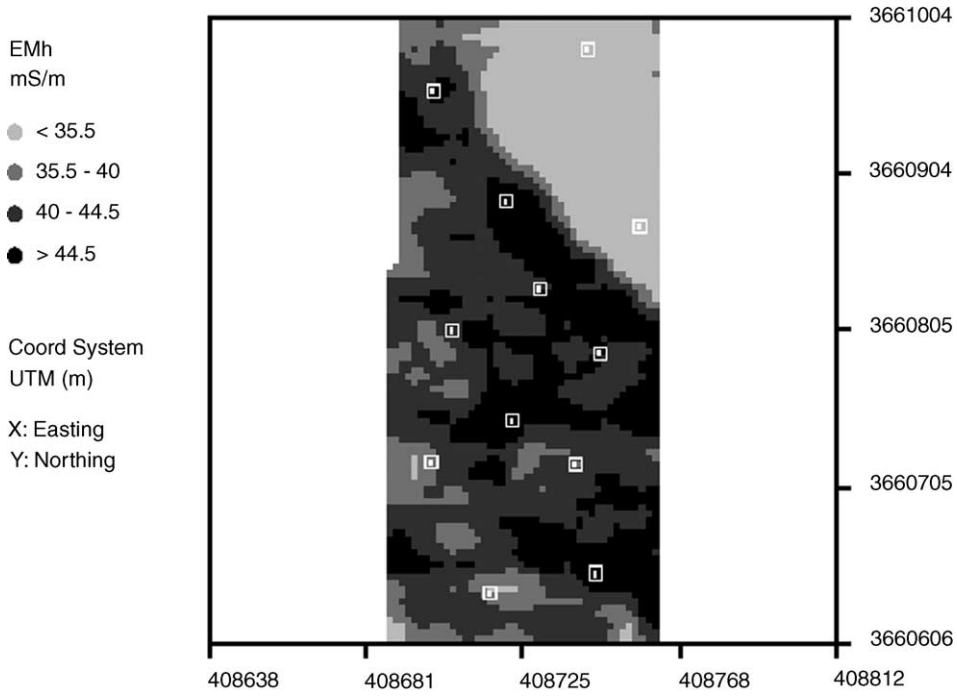

Fig. 5. Observed EM_H signal pattern in Field M22, with the 12 calibration sample site locations identified.

Table 6
Calibration soil salinity and texture summary statistics for Field M22

Soil property	Depth level (cm)	Mean	Standard deviation	Minimum	Maximum
EC_e (dS/m)	0–90	0.852	0.168	0.617	1.144
Clay (%)	0–90	23.00	5.92	10.62	32.34
Sand (%)	0–90	65.88	8.33	51.88	84.88
Silt (%)	0–90	11.12	2.84	4.49	15.78

Soil texture	Depth level (cm)	Casa Grande series		Mohall series	
		Mean	Standard deviation	Mean	Standard deviation
Soil texture classification by soil series					
Clay (%)	0–90	24.50	4.78	16.41	5.28
Sand (%)	0–90	64.20	6.50	72.55	10.85
Silt (%)	0–90	11.30	2.24	11.03	5.67

	Clay (%)	Sand (%)	Silt (%)
Soil texture correlation matrix (pooled across both soil series)			
Clay (%)	1.000	−0.977	0.784
Sand (%)		1.000	−0.897
Silt (%)			1.000

Table 6 shows the calibration soil sample summary statistics associated with this survey. These statistics again include the mean, standard deviation, minimum and maximum levels for the measured soil salinity (EC_e; dS/m) and soil texture (% clay, % sand, % silt) data from the 0–90 cm sampling depth. The EC_e data show that Field M22 is uniformly non-saline. In contrast, the soil texture data exhibit a fair amount of variability, particularly with respect to the % clay and % sand measurements. The mean % clay and % sand levels also exhibit distinct differences across soil series, with the Mohall series displaying higher % sand and lower % clay levels. The pooled soil texture correlation matrix indicates that the % sand and % clay sample data are inversely related ($r = -0.98$).

At this study site, the goal was to predict one or more of the soil texture properties from the corresponding EM survey data. Thus, Eq. (1) was initially fit to the calibration soil texture data with the trend surface variables defined to be the re-scaled UTM coordinate locations of the sample sites. A preliminary analysis of this model revealed that the residual independence assumption was reasonable. However, the estimated % silt model was found to be non-significant ($F = 2.41$, $p = 0.146$). Additionally, neither the trend surface parameters nor the vertical signal data were found to be statistically significant and/or improve the predictions in the clay and sand models. Thus, a new set of simple linear regression equations were refit to the % clay and % sand data using only the EM_H signal data.

The final set of estimated M22 regression equations are shown in Table 7. The R^2 and root mean square error estimates for the % clay and % sand models are 0.761, 3.04%, and 0.741, 4.44%, respectively. These R^2 estimates suggest that the EM_H signal data explains about 75% of the apparent clay and sand textural variation in this field.

Table 8 displays the field average summary statistics derived from these fitted regression models. The soil texture in Field M22 is (on the average) comprised of 23.2% clay and

Table 7
Regression model summary statistics for Field M22

	% Clay model (0–90 cm)	% Sand model (0–90 cm)
R^2	0.761	0.741
MSE	9.23	19.74

Variable	Estimate	Standard error	*t*-Score	Prob > |*t*|
Parameter estimates ($E(y) = \beta_0 + \beta_1 EM_H$)				
Clay (%)				
β_0	−3.84	4.84	−0.79	0.446
β_1	0.67	0.12	5.64	<.001
Sand (%)				
β_0	103.16	7.08	14.57	<.001
β_1	−0.93	0.18	−5.35	<.001

65.6% sand. Additionally, an estimated 80.5% of the field contains between 15% and 30% clay, and 61.5% of the field contains between 60% and 75% sand.

The 0–90 cm depth predicted % clay map is shown in Fig. 6. (The corresponding % sand map is not shown, since it is inversely proportional to the % clay map.) The spatial pattern in this map just reflects the original EM_H signal pattern, re-calibrated via the regression model into corresponding % clay levels. Not surprisingly, this map confirms that the low conductivity zone in the north–east area of M22 corresponds to a lower clay (higher sand) area (i.e., the Mohall soil series).

4.3. Tile line mapping (Field IV376)

Table 9 presents the EM_V signal data summary statistics for both surveys performed in Field IV376, while Fig. 7a and b show the corresponding spatial maps. The EM_V signal readings were about 30 mS/m higher in the July 2002 survey, but the relative spatial patterns are very similar. Both survey maps show the effect of a diagonal buried canal running

Table 8
Field average prediction statistics for Field M22

Depth (cm)	Soil texture (%)	Mean (95% CI)
Predicted field mean levels		
0–90	Clay	23.2 (21.3, 25.2)
0–90	Sand	65.6 (62.7, 68.4)

Range (%)	Clay (% of field)	Range (%)	Sand (% of field)
Predicted 0–90 cm field range interval estimates (with standard errors)			
<15	9.4 (3.4)	<60	25.1 (6.5)
15–20	16.9 (3.4)	60–65	26.0 (4.9)
20–25	32.7 (4.6)	65–70	22.0 (4.1)
25–30	30.9 (7.7)	70–75	13.5 (2.6)
>30	10.1 (2.8)	>75	13.4 (5.7)

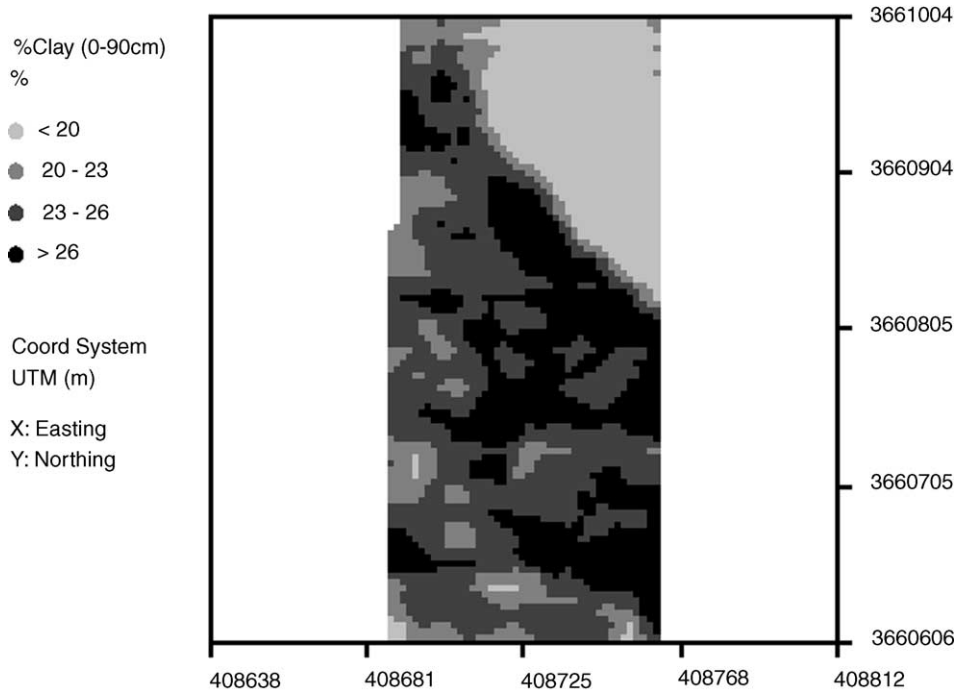

Fig. 6. Predicted % clay map (0–90 cm) for Field M22.

across the north–east part of the field. Both maps also exhibit pronounced anisotropic signal patterns, with the EM_V signal levels periodically rising and falling in a north–south direction across the field.

This oscillating conductivity pattern is plainly evident in the individual EM_V transect data. Fig. 8 shows the acquired July 2002 EM_V signal readings collected down transect #5,

Table 9
EM38 vertical signal summary statistics for Field IV376, August 2001 and July 2002 survey dates

	August 2001	July 2002
	EM_V (mS/m)	EM_V (mS/m)
N	7469	5603
Mean	198.13	229.48
Standard deviation	54.64	56.81
Quantiles		
Minimum	50.0	77.0
q10	125.0	151.0
q25	164.0	191.0
Median	197.0	232.0
q75	234.0	268.0
q90	269.0	302.0
Maximum	385.0	399.0

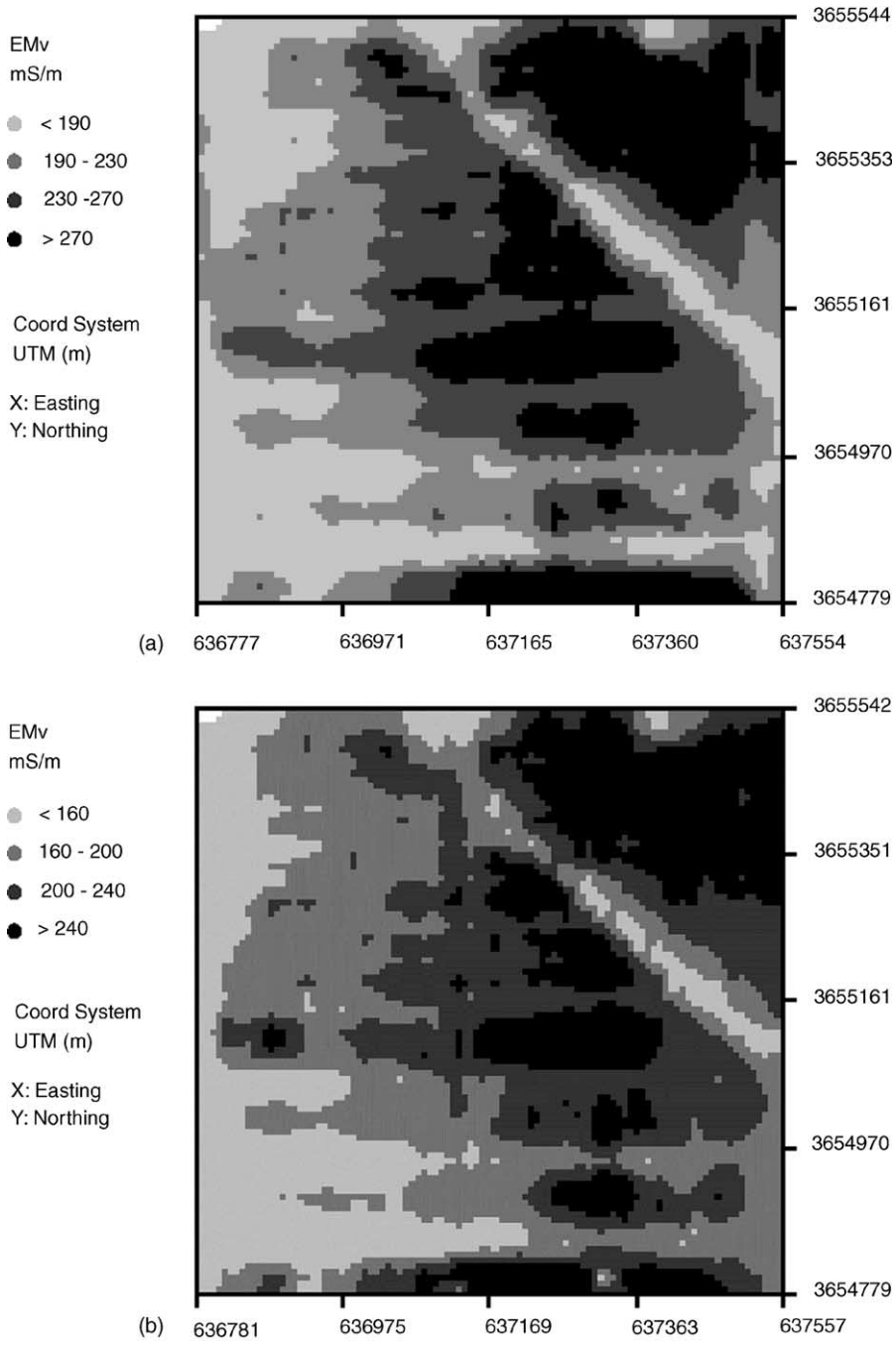

Fig. 7. Observed: (a) July 2002 and (b) August 2001 EM_V signal patterns in Field IV376.

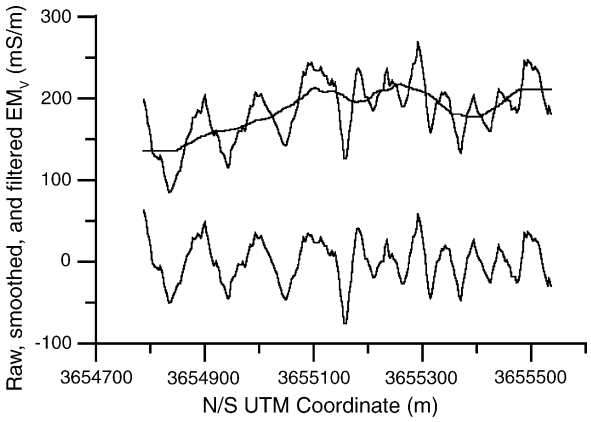

Fig. 8. Raw, smoothed, and filtered EM_V signal data from transect #5 in Field IV376; July 2002 survey.

located about 120 m from the west edge of the field. The upper cyclic plot represents the raw EM_V signal data, while the smoother line running through these readings represents the moving average calculated using a 60-m window. The lower cyclic plot represents the "filtered" EM_V data; i.e., the raw-smoothed differences. This latter pattern reveals at least 10 local minimums in the filtered data, with three below the UTM coordinate 3655100 N and seven above this coordinate location. Given the reasonable assumption that this filtered signal data reflects deviations in the soil salinity levels induced by water content variation and long-term differential leaching, each local minimum within this pattern represents a probable tile line location.

Fig. 9 displays a two-dimensional map of the filtered EM_V signal data. The effects of both the tile lines and (diagonal) buried canal are much more apparent in this image. The four southern tile lines now stand out clearly, and the northern tile line effects are also more readily visible.

In order to identify the tile line locations in the July 2002 filtered data, we first created a two-dimensional plot of all identified local minimums. These local minimums are referred to here as "draw-down points" (DDPs). This pattern is shown in Fig. 10a. Using this starting pattern, all DDPs that had absolute values less than 15% of the maximum identified DDP value were temporarily removed from the plot. Additionally, all DDPs that were not associated with at least two adjacent negative filtered EM_V readings (to either side of the DDP location) were also temporarily removed from the plot. These two pattern enhancement operations resulted in Fig. 10b, where the 10 tile lines are now clearly evident. We then threaded the 10 line positions, identified all DDPs within 8 m of each threaded line (including those points temporarily removed), and associated the correct tile line number with each identified DDPs. Fig. 10c shows the final identified 10 tile lines, and corresponding associated 210 DDPs.

The numbering system used for the 10 tile lines (as shown in Fig. 10c) was chosen to facilitate the ANOCOVA modeling analysis. Specifically, the installation records indicated that the southern lines were twice as far apart as the northern lines, so this tile line pattern

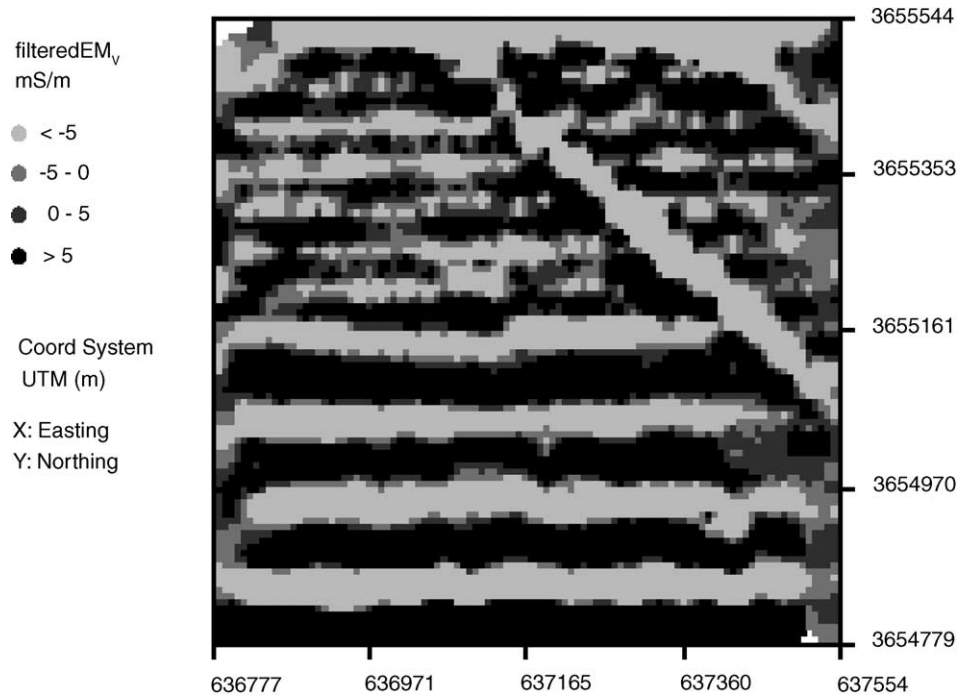

Fig. 9. Filtered July 2002 EM_V signal data, revealing locations of multiple tile lines and one diagonal buried canal in Field IV376.

should be discernable using either of the following statistical models:

$$y = \alpha_j + \beta_1[x] \quad \text{for} \quad j = 1, 2, \cdots, 10 \tag{11}$$

or,

$$y = \beta_0 + \beta_1[x] + \beta_2[N_{\mathrm{TL}}] \tag{12}$$

where (y) and (x) again represent appropriately re-scaled UTM coordinates, and N_{TL} represents the assigned tile line numbers shown in Fig. 10c. Eq. (11) represents a standard ANOCOVA model which allows for (possibly) different spacing between lines, while Eq. (12) represents the more restrictive assumption of an a priori known spacing scheme. Since Eq. (12) is nested within Eq. (11), a general F-test can be performed to determine which model provides the most parsimonious fit to the data (Weisberg, 1985).

When both of the above defined models were fit to the July 2002 DDP data, the corresponding nested-model F-test value was calculated to be $F = 1.51$ ($p = 0.155$). Thus, Eq. (12) was judged to be adequate, and used to estimate the 10 tile line positions. The summary statistics and parameter estimates for this model are shown in Table 10. The model produced an R^2 value of 0.9999, a mean square error (MSE) estimate of 3.86 m, and a calculated split-line spacing of 53.23 m. This β_2 parameter estimate closely agrees with the

recorded split-line spacing of 53.34 m, and the general model summary statistics suggest that the 10 tile line positions have been accurately defined.

To test the repeatability of this tile line mapping methodology, we performed an identical type of analysis on the IV376 August 2001 EM_V survey data. As before, we smoothed and filtered the EM_V data, visually located and threaded the same 10 tile lines, and in this analysis identified 285 distinct DDPs (associated with the 10 lines). Eqs. (11) and (12) were then re-estimated using this new data, and a nested-model F-test statistic ($F = 1.73$,

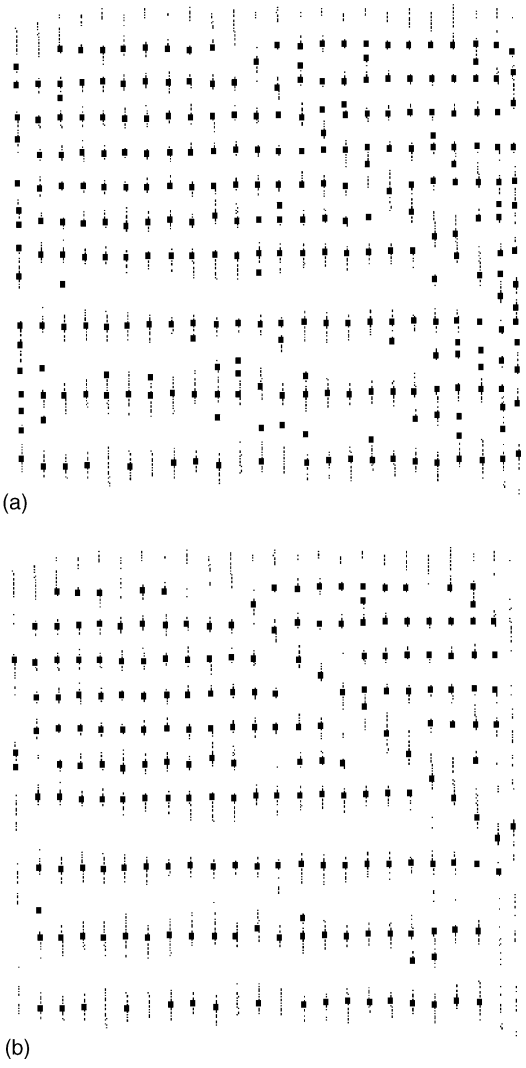

Fig. 10. (a) The complete set of draw down points (DDPs) identified from the July 2002 EMV signal data in Field IV376; (b) a reduced set of DDPs that more clearly show the 10 tile line positions; and (c) the final set of DDPs associated with each of the 10 identified tile lines in Field IV376.

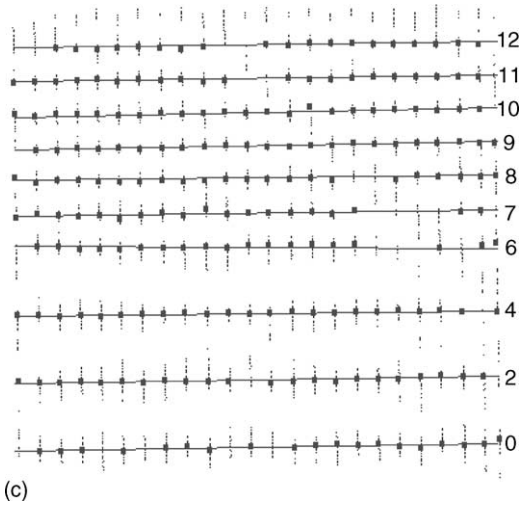

Fig. 10. (*Continued*).

$p = 0.092$) was calculated. This test result again suggested that Eq. (12) was appropriate. The corresponding model summary statistics and parameter estimates corresponding to the August 2001 survey data are also shown in Table 10, respectively. This second model produced an R^2 value of 0.9998, a MSE estimate of 6.72 m, and a calculated split-line spacing of 53.31 m.

Finally, the DDP data from both surveys were pooled together in order to test the equivalence of the two sets of parameter estimates. The calculated *F*-test value corresponding to the hypothesis of equivalent parameter estimates was $F = 4.98$ ($p = 0.002$). This result suggests that these two sets of parameter estimates are *statistically* different (specifically, the β_0 and β_1 estimates appear to be different across the two surveys). However, this test does not quantify the magnitude of deviation between the mapped tile line locations across the two

Table 10
Tile line regression model summary statistics for Field IV376, August 2001 and July 2002 survey dates

	July 2002 model ($N = 210$ DDPs)	August 2001 model ($N = 285$ DDPs)
R^2	0.9999	0.9998
MSE	3.86	6.72
Parameter estimates (with standard errors)[a]		
β_0	135.41 (0.40)	136.57 (0.46)
β_1	0.0140 (0.0006)	0.0114 (0.0007)
β_2	53.23 (0.037)	53.31 (0.041)
95% confidence interval for apparent tile line spacing (m)		
	(53.16, 53.31)	(53.23, 53.39)

[a] The equation form is ($y = mx + b$), and the prediction, model is defined as a function of both X and the tile line number (N_{TL}); i.e., $Y - Ys = \beta_0 + \beta_1[X - Xs] + \beta_2[N_{TL}]$, where the X/Y shift factors are ($Xs = 636{,}700$, $Ys = 3{,}654{,}700$) and the N_{TL} values are shown in Fig 10c.

survey dates. In order to accurately quantify this, the *y*-positions of each line along both the eastern and western edges of the field were estimated using the time specific Eq. (12) models (using UTM *x*-coordinates approximately 50 m in from the eastern and western field boundaries). The absolute difference between the predicted 20 *y*-coordinates were then calculated for the two survey dates, and subsequently analyzed. The average absolute difference was found to be 0.94 m, and the minimum and maximum observed absolute differences (out of all 20 values) were 0.03 and 1.85 m, respectively. Thus, the average absolute difference in the predicted set of tile line locations as derived from these two EM surveys was found to be <1 m. This estimate coincides with the stated accuracy of the Trimble differential GPS system used during the data collection process.

5. Conclusion

Spatial salinity mapping using EM survey data has been well documented in the soil literature. However, this technology has steadily evolved from a basic mapping procedure into a more comprehensive tool for supplying detailed feedback on various agricultural management practices. In the CV5 leaching example, this feedback represents the change (or lack there of) in the spatial salinity pattern attributable to the leaching event. More specifically, these survey data show that the leaching event has basically failed; the highest saline areas mapped in CV5 show virtually no change between the pre- versus post-leaching time frames.

The soil texture mapping in Field M22 represents a more traditional soil property mapping example. In this particular study, the spatial soil texture information was needed as input to a spatially referenced cotton production model. However, this information can be used for many diverse purposes, such as better defining the NRCS soil mapping boundary zone between the Mohall sandy loam and Casa Grande clay loam soil series.

More importantly, the same general statistical methodology was used to produce both the CV5 salinity maps and M22 texture map. This latter point deserves emphasis; the regression-based statistical modeling and prediction approach discussed here is very general. Provided the EM survey data is well correlated with the soil property of interest, accurate quantification and prediction of that soil property is usually possible using this approach.

The tile line mapping example in Field IV376 represents a more recent application of EM surveying technology. In many fields, permanently installed tile lines result in long-term preferential leaching patterns that are directly reflected in the EM signal data response pattern. When such cyclic patterns are detected, the data can be used to accurately map the positions of the detected lines. As shown in this example, the average error in the repeatability of the tile line mapping process (<1 m) was equivalent to the manufacturer stated position uncertainty in the GPS location data. This surveying technique can be very useful when the exact locations of the individual lines are not known (as is often the case with older drainage systems). Tile lines requiring maintenance or cleaning may also be detected during these surveys, since damaged or clogged lines often cause abrupt changes in the preferential leaching pattern.

In summary, the preceding case studies demonstrate some of the current applications for agricultural EM survey work in the arid southwestern United States. Although each application is different, the underlying technology is the same. These projects demonstrate that diverse types of spatial information can be derived from EC_a survey data, and that this information can be readily used to help improve the overall management of agricultural fields.

Acknowledgments

D.A. Robinson was in part funded by a USDA NRI grant (2002-35107-12507) while undertaking this research. The authors also wish to acknowledge and thank Donald Ackley (Coachella Valley Water District) and Steve Burch (Imperial Irrigation District) for assisting in the collection of the EM survey data in fields CV5 and IV376, respectively.

References

Carter, L.M., Rhoades, J.D., Chesson, J.H., 1993. Mechanization of soil salinity assessment for mapping. In: ASAE Winter Meetings, 12–17 December. Chicago, IL. ASAE, St. Joseph, MI, USA (ASAE Paper No. 931557).

Cook, R.D., Weisberg, S., 1999. Applied Regression Including Computing and Graphics. John Wiley, NY, USA.

Corwin, D.L., Lesch, S.M., 2003. Application of soil electrical conductivity to precision agriculture: theory, principles, and guidelines. Agron. J. 95, 455–471.

Doolittle, J.A., Sudduth, K.A., Kitchen, N.R., Indorante, S.J., 1994. Estimating depths to claypans using electromagnetic induction methods. J. Soil Water Conserv. 49, 572–575.

Graybill, F.A., 1976. Theory and Application of the Linear Model. Wadsworth Publishing Co., Inc., Belmont, CA, USA.

Hendrickx, J.M.H., Baerends, B., Raza, Z.I., Sadig, M., Chaudhry, M.A., 1992. Soil salinity assessment by electromagnetic induction of irrigated land. Soil Sci. Soc. Am. J. 56, 1933–1941.

Jaynes, D.B., Colvin, T.S., Ambuel, J., 1993. Soil type and crop yield determinations from ground conductivity surveys. ASAE Paper No. 933552. ASAE, St. Joseph, MI, USA.

Johnson, C.K., Mortensen, D.A., Wienhold, B.J., Shanahan, J.F., Doran, J.W., 2003. Site-specific management zones based upon soil electrical conductivity in a semiarid cropping system. Agron. J. 95, 303–315.

Kachanoski, R.G., Gregorich, E.G., Van-Wesenbeeck, I.J., 1988. Estimating spatial variations of soil water content using noncontacting electromagnetic inductive methods. Can. J. Soil Sci. 68, 715–722.

Kitchen, N.R., Sudduth, K.A., Drummond, S.T., 1999. Soil electrical conductivity as a crop productivity measure for claypan soils. J. Prod. Agric. 12, 607–617.

Kitchen, N.R., Sudduth, K.A., Drummond, S.T., 1996. Mapping of sand deposition from 1993 Midwest floods with electromagnetic induction measurements. J. Soil Water Conserv. 51, 336–340.

Lesch, S.M., 2005. Sensor-directed response surface sampling designs for characterizing spatial variation in soil properties. Comput. Electron. Agric. 46, 153–179.

Lesch, S.M., Corwin, D.L., 2003. Predicting EM/soil property correlation estimates via the Dual Pathway Parallel Conductance model. Agron. J. 95, 365–379.

Lesch, S.M., Rhoades, J.D., Corwin, D.L., 2000. ESAP-95 Version 2.10R: User Manual and Tutorial Guide. Research Rpt. 146. USDA-ARS George E. Brown Jr. Salinity Laboratory, Riverside, CA, USA.

Lesch, S.M., Strauss, D.J., Rhoades, J.D., 1995a. Spatial prediction of soil salinity using electromagnetic induction techniques. Part 1. Statistical prediction models: a comparison of multiple linear regression and cokriging. Water Resour. Res. 31, 373–386.

Lesch, S.M., Strauss, D.J., Rhoades, J.D., 1995b. Spatial prediction of soil salinity using electromagnetic induction techniques. Part 2. An efficient spatial sampling algorithm suitable for multiple linear regression model identification and estimation. Water Resour. Res. 31, 387–398.

Littell, R.C., Milliken, G.A., Stroup, W.W., Wolfinger, R.D., 1996. SAS system for Mixed Models. SAS Institute Inc., Cary, NC, USA.

McNeill, J.D., 1980. Electromagnetic Terrain Conductivity Measurement at Low Induction Numbers, Tech. Note TN-6. Geonics Limited, Ont., Canada.

Myers, R.H., 1986. Classical and Modern Regression with Applications. Duxbury Press, Boston, MA, USA.

Plant, R.E., 2001. Site-specific management: the application of information technology to crop production. Comput. Electron. Agric. 30, 9–29.

Press, S.J., 1989. Bayesian Statistics: Principles, Models, and Applications. John Wiley, NY, USA.

Rhoades, J.D., 1992. Instrumental field methods of salinity appraisal. In: Topp, G.C., Reynolds, W.D., Green, R.E. (Eds.), Advances in Measurement of Soil Physical Properties: Bring Theory into Practice. SSSA Special Publication No. 30. Soil Science Society of America, Madison, WI, USA, pp. 231–248.

Rhoades, J.D., 1996. Salinity: Electrical conductivity and total dissolved salts. In: Sparks, D.L. (Ed.), Methods of Soil Analysis. Part 3—Chemical Methods. Soil Science Society of America Book Series 5. Soil Science Society of America, Madison, WI, USA, pp. 417–435.

Rhoades, J.D., Manteghi, N.A., Shouse, P.J., Alves, W.J., 1989. Soil electrical conductivity and soil salinity: new formulations and calibrations. Soil Sci. Soc. Am. J. 53, 433–439.

Rhoades, J.D., Chanduvi, F., Lesch, S.M., 1999. Soil salinity assessment: methods and interpretation of electrical conductivity measurements. FAO Irrigation and Drainage Paper #57. Food and Agriculture Organization of the United Nations, Rome, Italy, 1–150.

Rhoades, J.D., Lesch, S.M., LeMert, R.D., Alves, W.J., 1997. Assessing irrigation/drainage/salinity management using spatially referenced salinity measurements. Agric. Water Manag. 35, 147–165.

Royle, J.A., Berliner, M., 1999. A hierarchical approach to multivariate spatial modeling and prediction. J. Agric. Biol. Environ. Stat. 4, 29–56.

SAS Institute Inc., 1999. SAS/STAT User's Guide, Version 8. SAS Institute Inc., Cary, NC, USA.

Sheets, K.R., Hendrickx, J.M.H., 1995. Non-invasive soil water content measurement using electromagnetic induction. Water Resour. Res. 31, 2401–2409.

Sudduth, K.A., Kitchen, N.R., Hughes, D.F., Drummond, S.T., 1995. Electromagnetic induction sensing as an indicator or productivity on claypan soils. In: Robert, P.C., Rust, R.H., Larson, W.E. (Eds.), Proceedings of the Second International Conference on Site-Specific Management for Agricultural Systems. ASA-CSSA-SSSA, Madison, WI, USA, pp. 671–681.

Thompson, S.K., 1992. Sampling. John Wiley, NY, USA.

Triantafilis, J., Huckel, A.I., McBratney, A.B., 1998. Estimating deep drainage on the field scale using a mobile EM sensing system and Sodium-SaLF. In: Proceedings of the Ninth Australian Cotton Growers Research Association Conference, August 12–14, 1998, Broadbeach, Queensland, Australia, pp. 61–64.

United States Department of Agriculture, 1984. Soil survey of Pinal County, Arizona: western part. Soil Conservation Service, Washington, DC, USA.

United States Department of Agriculture, 1980. Soil survey of Riverside County California: Coachella Valley Area. Soil Conservation Service, Washington, DC, USA.

Weisberg, S., 1985. Applied Linear Regression, second ed. John Wiley, NY, USA.

Williams, B.G., Baker, G.C., 1982. An electromagnetic induction technique for reconnaissance surveys of soil salinity hazards. Aust. J. Soil Res. 20, 107–118.

Williams, B.G., Hoey, D., 1987. The use of electromagnetic induction to detect the spatial variability of the salt and clay contents of soils. Aust. J. Soil Res. 25, 21–27.